

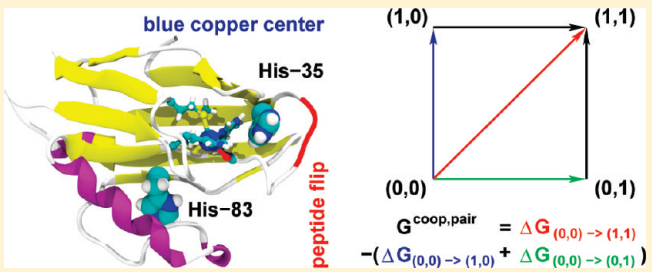
# Coupling of Protonation, Reduction, and Conformational Change in azurin from *Pseudomonas aeruginosa* Investigated with Free Energy Measures of Cooperativity

R. Thomas Ullmann\* and G. Matthias Ullmann\*

Structural Biology/Bioinformatics, University of Bayreuth, Universitätsstrasse 30, BGI, 95447 Bayreuth, Germany

S Supporting Information

**ABSTRACT:** We used free energy calculations within a continuum electrostatics model to analyze the coupling of protonation, reduction, and conformational change in azurin from *Pseudomonas aeruginosa* (PaAz). PaAz was characterized extensively with a variety of experimental methods. Experimentally determined pK<sub>a</sub> values and pH-dependent reduction potentials are used to validate our computational model. It is well-known from experiment that the reduction of the copper center is coupled to the protonation of at least two titratable residues (His-35 and His-83) and to the flip of the peptide bond between Pro-36 and Gly-37. Free energy measures of cooperativity are used for a detailed analysis of the coupling between protonation, reduction, and conformational change in PaAz. The reduction of the copper center, the protonation of His-35, and peptide flip are shown to be cooperative. Our results show that cooperativity free energies are useful in detecting and quantifying thermodynamic coupling between events in biomolecular systems. The protonation of His-35 and the peptide flip are found to be so tightly coupled that these events happen effectively concerted. This concerted change results in a marked alteration of the electrostatic surface potential of azurin that might affect the interaction of azurin with its binding partners.



## 1. INTRODUCTION

Azurin from *Pseudomonas aeruginosa* (*P. aeruginosa*, PaAz) is a small electron-transport protein with a blue copper center.<sup>1,2</sup> The structure of PaAz is shown in Figure 1. The exact physiological role of PaAz and the identity of its electron-transfer partners are not yet known.<sup>3</sup> PaAz has been shown to be able to exchange electrons with cytochrome *c*<sub>551</sub>, cytochrome *cd*<sub>1</sub> nitrite reductase, and the cytochrome *bc*<sub>1</sub> complex of *P. aeruginosa*.<sup>3,4</sup> Experiments with knockout mutants could not yet identify, however, an essential role for PaAz, at least under the conditions studied.<sup>3</sup> Electron transfer with all known possible redox partners can also be fulfilled by other electron carriers such as cytochrome *c*<sub>551</sub>.<sup>3,4</sup> The understanding of the respiratory system of *P. aeruginosa* is also of medical interest, because this bacterium occurs as opportunistic pathogen in human diseases such as cystic fibrosis.<sup>5,6</sup> Such understanding could aid in the search for potent drugs against *P. aeruginosa*. The search for such drugs is especially important, because strains of the bacterium appeared among the multidrug-resistant pathogens that have become a major problem in medicine.<sup>5,6</sup>

In the past years, PaAz has found renewed interest as a potential therapeutic agent against cancer cells,<sup>7</sup> malaria pathogens, and HIV.<sup>8</sup> The basis for such applications is the ability of PaAz to induce apoptosis in mammalian cells.<sup>7</sup> This ability is independent of its redox activity<sup>9</sup> and depends on the interaction of PaAz with the mammalian tumor suppressor p53.<sup>7,10</sup> *P.*

*aeruginosa* has been found to secrete PaAz and cytochrome *c*<sub>551</sub> into the surrounding medium.<sup>7</sup> From there, these bacterial redox proteins are taken up by mammalian cells (preferentially cancer cells)<sup>11</sup> and induce apoptosis.<sup>7</sup> The antimalaria and anti-HIV activities of PaAz seem to be based on a prevention of pathogen entry into the mammalian cell.<sup>8</sup> For these reasons, it has been proposed that the cytotoxic capacity of PaAz and its antimalaria and anti-HIV activities may have evolved as a defense against predators or concurrents for the same nutrients in an infected host.<sup>7,8</sup>

PaAz was characterized extensively with a variety of experimental methods. Experimentally determined pK<sub>a</sub> values and pH-dependent reduction potentials are compared to our results to validate our computational model of this system. It is well-known from experiment that the reduction of the copper center is coupled to the protonation of at least two titratable residues (His-35 and His-83) and to the flip of the peptide bond between Pro-36 and Gly-37.<sup>12–16</sup> Azurin from *Alcaligenes denitrificans* (*A. denitrificans*) has been used as a model system in an early continuum electrostatic study on the effect of metal oxidation on the pK<sub>a</sub> values of protein residues.<sup>17</sup> We use azurin for a case study to show that free energy measures of cooperativity are useful for analyzing the coupling between events in biomolecular

Received: May 18, 2011

Revised: July 14, 2011

Published: July 20, 2011

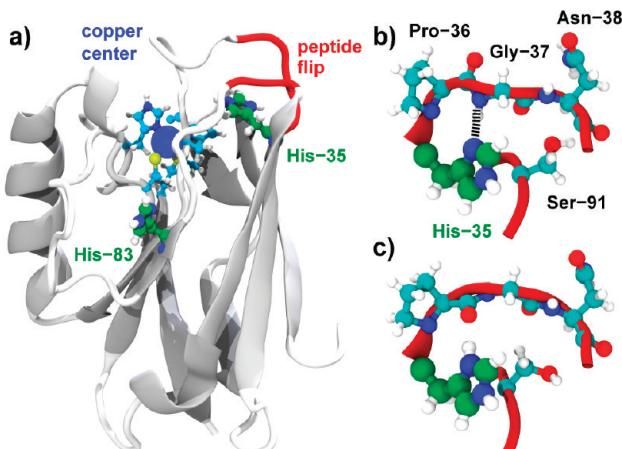


**Figure 1.** Structure of azurin from *Pseudomonas aeruginosa* (PaAz). The coupling of reduction and protonation<sup>20</sup> in PaAz involves the flip of the peptide bond plane between Pro-36 and Gly-37 that occurs between the pH values 5.5 and 9.0.<sup>12</sup> This peptide flip is tightly coupled to the protonation of His-35.<sup>16</sup> The protonation of the residues His-35 and His-83 is believed to cause the pH-dependence of the reduction potential of the copper center.<sup>13–16,21</sup> (a) Overall structure: the locations of the copper center, His-35, His-83, and the peptide flip region are indicated. (b) Structure of the peptide flip region at high pH values (PDB 5AZU):<sup>12</sup> His-35 is deprotonated. (c) Structure of the peptide flip region at low pH values (PDB 4AZU):<sup>12</sup> His-35 is protonated. The conformationally variable residues included in modeling the peptide flip region are Pro-36, Gly-37, Asn-38, and Ser-91 from the adjacent loop (indicated in panel b) in line with findings from NMR experiments.<sup>22</sup> The figure was prepared with VMD<sup>23</sup> and Tachyon.<sup>24</sup>

systems. Cooperativity free energies can be used to detect and quantify this thermodynamic coupling.<sup>18,19</sup> The coupling of protonation, reduction, and conformational change in azurin is analyzed in detail. Implications of our findings for the physiological function of PaAz and its application as therapeutic agent are discussed.

The parts of this paper are organized as follows. The next section specifies the computational methods employed in our calculations. Our results are presented and discussed in section 3. We close with a summary of our findings and the conclusions thereof.

## 2. METHODS

The work flow of our computational methods begins with structure preparation with the program CHARMM. In this stage, hydrogen atoms are added to the crystal structure and their positions are energy minimized. Rotamer positions for hydroxyl hydrogens and alternative positions of protons on carboxyl groups are also added. Atomic radii are assigned to each atom.

The next stage is performed by an in-house program<sup>25</sup> based on our modified version of the MEAD library.<sup>26,27</sup> In this stage, side chain rotamer positions, and different binding and charge forms are generated. Microscopic intrinsic energies and interaction energies between the sites are computed on the basis of a continuum electrostatics/molecular mechanics model.<sup>19</sup>

The last stage constitutes the productive phase. Equilibrium properties of PaAz are computed from Monte Carlo (MC) simulation data.<sup>19</sup> The MC simulations are based on a microstate description of the system.<sup>19,28,29</sup> This description is a refined version of earlier models of protonation and reduction equilibria

in proteins and other macromolecules that were developed and evolved in our and other groups.<sup>27,30–33</sup> Details of the underlying theory and its computational implementation are given in ref 19. The microscopic intrinsic energies and interaction energies calculated in the previous stage can be used to compute the microstate energy of our model system during the simulations. A microstate is defined by a particular instance occupied by each site. The term instance describes the combination of a particular set of atomic partial charges, a particular number of bound ligands of each ligand type (here electrons and protons), and a particular set of atomic coordinates. The energy of a microstate is given by<sup>19</sup>

$$E_n^{\text{micro}} = \sum_{i=1}^{N^{\text{sites}}} (E_{i,k}^{\text{int}} - \sum_m^{\mathcal{L}} \nu_{i,k,m} \bar{\mu}_m) + \sum_{i=1}^{N^{\text{sites}}} \sum_{j=1}^{j < i} W_{i,k,j,l} \quad (1)$$

where  $N^{\text{sites}}$  is the number of sites and  $\mathcal{L}$  is the number of ligand types.  $E_{i,k}^{\text{int}}$  is the intrinsic energy of site  $i$  in instance  $k$ . The stoichiometric coefficient  $\nu_{i,k,m}$  indicates the number of ligands of type  $m$  bound to instance  $k$  of site  $i$  and  $\bar{\mu}_m$  is the electrochemical potential of this ligand in the surrounding solution.  $W_{i,k,j,l}$  is the interaction energy of sites  $i$  and  $j$  in their respective instances  $k$  and  $l$ .

**Calculation of Parameters.** Partial charges for the T1 copper centers of azurins were obtained from density functional theory (DFT) calculations at a model system. The model system consisted of all side chain atoms of the coordinating residues His-46, Cys-112, His-117, and Met-121. For Gly-45, the coordinating carbonyl group was included. In addition, the backbone atoms connecting the coordinating residues His-46 and Gly-45 were included. The coordinates were taken from the PDB-entry 4AZU. Free valences were capped with hydrogen atoms. The DFT calculations were performed with the ADF program<sup>34</sup> (functionals VWN<sup>35</sup> and OPBE<sup>36</sup> with a TZ2P basis set). The atomic partial charges for the copper center were obtained with an in-house-modified version of the multipole-derived charge analysis method.<sup>37</sup> Our modifications allow one to include constraints in the charge fitting procedure, which were used to set the charge of link atoms to a value of zero.<sup>25</sup> The atoms included in the model of the copper site and their atomic partial charges are listed in Table S3 of the Supporting Information.

Four alternative hydrogen positions are constructed for protonated carboxylic acids representing syn and anti configurations for both protonatable oxygen atoms. The energy difference between syn and anti configurations was set to 2 kcal/mol on the basis of the upper bound for this value obtained from gas-phase DFT calculations with different functionals and basis sets. The geometric parameters for adding the dissociable hydrogen was adopted from the ideal gas phase geometry obtained for propionic acid with the PBE and VWN functionals. The DFT calculations were performed with the ADF program<sup>34</sup> (functionals VWN<sup>35</sup> and BP86<sup>38,39</sup> with a QZ4P basis set).

Atomic partial charges for forms of protonatable amino acids that were not available from the CHARMM force field were derived from DFT calculations. The DFT calculations were performed with the ADF program<sup>34</sup> (functionals VWN<sup>35</sup> and BP86<sup>38,39</sup> with a QZ4P basis set). Atomic partial charges for deprotonated arginine and lysine were fitted with the multipole-derived charge analysis.<sup>37</sup> The side chain analogues *n*-propylguanidine and *n*-butylamine were used for arginine and lysine, respectively. The intrinsic energies for the model compounds of deprotonated lysine were computed from the macroscopic

$pK_a$  value and a symmetry correction to account for the presence of three isoenergetic deprotonated forms.<sup>19,40</sup> The intrinsic energies for the model compounds of deprotonated arginine could not be simply computed from the macroscopic  $pK_a$  value of the model compounds, since the different tautomeric forms are not equivalent. The relative intrinsic energies of the tautomers were computed from their relative free energies in aqueous solution. The free energies of the model compounds were computed from DFT augmented with the electrostatic solvation. The DFT energy consisted of the single-point DFT energy and the vibrational energy in the gas phase. The electrostatic solvation energies were computed with the MEAD package.<sup>26,27</sup> The intrinsic energy difference relative to the protonated form was computed using the intrinsic energies of the deprotonated forms and the macroscopic  $pK_a$  value of arginine. The intrinsic model energies and atomic partial charges are listed in the Supporting Information.

**Structure Preparation and Continuum Electrostatics Calculations.** The structures of PaAz in the high-pH form (PDB code SAZU chain A) and in the low-pH form (PDB code 4AZU chain A) were used as the basis for our calculations.<sup>12</sup> Hydrogen atoms were added with HBUILD<sup>41</sup> in CHARMM<sup>42</sup> and subsequently minimized using the CHARMM force field.<sup>43</sup> The peptide flip region (see Figure 1) was modeled as one site consisting of Pro-36, Gly-37, Asn-38, and Ser-91. These residues were found to be the only residues that undergo a significant conformational change between the high-pH and the low-pH crystal structures.<sup>12</sup> This finding is in line with findings from NMR experiments, where the other parts of the protein were found to be very rigid.<sup>22</sup> Also molecular dynamics (MD) simulations in which all parts of the protein except the Cu site (see above) were free to move confirmed this finding (data not shown).

Four conformers of the peptide flip region were generated from 1 ns MD simulations of PaAz with CHARMM in explicit solvent. The simulations were performed for the high-pH and low-pH forms with the copper center oxidized and reduced. All protonatable residues except His-35 and His-83 were set to standard protonation states. His-83 was fully protonated. His-35 was fully protonated for the low-pH form and singly protonated at NE2 for the high-pH form (see Figure 1). The protein was embedded in the cubic box of TIP3P water molecules with a length of 90 Å. Explicit potassium and chloride ions were added at a concentration of  $\approx 0.15$  mol/L. The initial coordinates of the water box and the ions were generated with VMD.<sup>23</sup> The simulation was run at standard temperature (298.15 K) and pressure (1 atm). The particle-mesh Ewald method was used for the electrostatics part of the energy function. During the simulation all parts of the protein apart from the peptide flip region, including the Cu site, were fixed to allow a reinsertion of the resulting conformers into the same structure. The conformational energy of the peptide flip region was estimated from the average dihedral energy plus the internal nonbonded interactions during a 1 ns MD simulation of PaAz with CHARMM<sup>42</sup> using the CHARMM force field.<sup>43</sup> The coordinates of the conformers were taken from the energy-minimized, average structure of each simulation. During the energy minimization, the coordinates of all other parts of the protein remained fixed and the dihedral angles of the peptide flip region were restrained with a harmonic potential using a force constant of 20.0 kcal/(mol rad<sup>2</sup>).

The intrinsic energies and interaction energies were computed with a continuum electrostatics/molecular mechanics model

within our in-house version<sup>25</sup> of the MEAD package.<sup>26,27</sup> The underlying theory is detailed in ref 19. All aspartate, histidine, glutamate, lysine, arginine, and tyrosine residues were considered as protonatable sites except for the copper ligands His-46 and His-117. The copper center was considered a redox-active site with an oxidized form and a reduced form. Side chain rotamers were added for flexible amino acid residues on the protein surface. The residues considered were Glu-2, Asp-6, Gln-8, Asn-18, Asp-23, Lys-24, Ser-25, Lys-27, Ser-34, Leu-39, Lys-41, Asp-55, Asp-62, Met-64, Asp-69, Lys-70, Asp-71, Lys-74, Asp-76, Asp-77, Arg-79, Lys-85, Glu-91, Lys-92, Asp-93, Asp-98, Lys-101, Lys-103, Glu-104, Glu-106, Gln-107, Lys-122, and Lys-128. Side chain rotamers were generated using the side chain dihedral angles from the backbone-dependent Squirrel rotamer library.<sup>44</sup> Conformational energies of side chain rotamers were computed using the CHARMM22 force field,<sup>43</sup> where we used dihedral energy terms, internal electrostatic energies within the site, and Lennard-Jones interaction energies within the site and between the site and the background (i.e., parts of the protein not belonging to any site). Lennard-Jones interactions were also added to the site–site interaction energies. The effect of the Lennard-Jones potential contribution to the site–site interaction energies is mainly the adding of a penalty for clashes between rotamers of flexible sites and other parts of the protein. The calculation of the electrostatic contributions to the intrinsic energies and interaction energies is described below.

We used a detailed charge model with explicit hydrogen positions for all protonatable sites. Atomic partial charges for standard forms of amino acid residues were taken from the CHARMM22 parameter set.<sup>43</sup> Atomic partial charges of nonstandard forms of amino acid residues and the copper center were obtained from DFT calculations (see above). Model compounds of protonatable amino acids include the entire residue plus the directly neighboring CHARMM charge groups belonging to the backbone of the preceding and succeeding amino acids to ensure charge neutrality and to mimick an *N*-formyl, *N*-methylamide blocked amino acid compounds.<sup>45</sup> The model compound for the copper center includes the copper ion, the backbone carbonyl group of Gly-45, and all side chain atoms of the ligating amino acids His-46, Cys-112, His-117, and Met-121. The intrinsic energies of the model compounds for protonatable amino acid residues in aqueous solution were calculated from  $pK_a$  values of appropriate model compounds taken from the literature<sup>32,46</sup> (see the Supporting Information). The intrinsic energies for the model compound of the copper center were fitted by matching the calculated midpoint potential of azurin from *A. denitrificans* to the experimental value of 278 mV.<sup>15</sup> The fitting was carried out on a static structure without side chain rotamers. The obtained intrinsic energy for the model compound in water is 13.3 kcal/mol for the oxidized form relative to the reduced form.

MEAD uses a finite-difference method on cubic grids to solve the linearized Poisson–Boltzmann equation. The dielectric constant of the protein was set to 4, and that of the solvent was set to 80.<sup>27</sup> The temperature was set to 298.15 K. The dielectric boundary between solute and solvent was calculated using a water probe sphere of 1.4 Å radius and the atomic radii (1.0 Å for H, 1.55 Å for N, 1.7 Å for C, 1.5 Å for O, 1.8 Å for S, and 1.3 Å for Cu). The ionic strength was set to 0.15 M. The thickness of the ion exclusion layer was set to 2.0 Å. Electrostatic potentials were computed using the focusing technique<sup>47</sup> with three cubic grids. The grids had grid spacings of 2.0, 0.5, and 0.2 Å, respectively.

The outer grid had a grid length of 101 points and was centered on the geometric center of the protein. The middle grid had a grid length of 201 points and was centered on the geometric center of the site. The inner grid had a grid length that was adjusted for each instance of each site separately to fit the dimensions of the site plus 15 Å in each direction and was centered on the geometric center of the site. The same grids were used for the model compound and the site in the protein.

In continuum electrostatics calculations with side chain rotamers, the dielectric boundary of the protein has to be approximated by assuming the presence of all rotameric forms of all sites other than the immediate site of interest at the same time.<sup>48</sup> As a consequence of the increased low-dielectric volume, electrostatic interaction energies are overestimated. To reduce the associated error, the number of side chain rotamers is reduced. First, all rotamers with large unfavorable Lennard-Jones interactions due to clashes with the background were removed. After a first calculation of the continuum electrostatics contributions to the intrinsic energies, the number of rotamers was further reduced with a modified version of the Goldstein criterion.<sup>49</sup> The modified Goldstein criterion uses an energy cutoff  $C$  to retain low-energy rotamers that could be thermally accessible. Each rotamer of site  $i$  can occur in multiple instances  $k$ . All rotamers of site  $i$  for which all instances  $k$  belonging to the rotamer fulfill

$$E_{i,k}^{\text{int}} - E_{i,k'}^{\text{int}} + \sum_{j \neq i} \min_l [W_{i,k,j,l} - W_{i,k',j,l}] > C \quad (2)$$

are removed. Here, the sum runs over the most favorable interaction energies  $W_{i,k,j,l}$  of site  $i$  in instance  $k$  with all other sites  $j$  in instance  $l$ . The reference instance  $k'$  of site  $i$  is determined via

$$k' = \arg \min_k [E_{i,k}^{\text{int}} + \sum_{j \neq i} \min_l [W_{i,k,j,l}]] \quad (3)$$

Multiple refinement cycles of the continuum electrostatics calculations were performed with an increasingly tight cutoff criterium. The final cutoff was set to  $C = 6.0$  kcal/mol.

**Monte Carlo Simulations.** All MC simulations were carried out with our program suite GMCT.<sup>19</sup> The temperature was set to 298.15 K. The interaction energy cutoff for pair and triplet moves were set to 0.5 kcal/mol and 1.0 kcal/mol, respectively.

Macroscopic binding properties were calculated with the Wang–Landau MC method.<sup>50</sup> A constant energy bin width of 0.1 kcal/mol was used for the energy histograms and the number of microstates. The initial modification factor  $f$  for the number of microstates was set to 2.0. The modification factor was decreased every 20 000 MC scans if the histogram flatness was improved or stayed equal relative to the last check. The modification factor was decreased according to the recursion formula  $f_{i+1} = f_i^{1/1.005}$  until it fell below a minimum value of 1.000 0005. The histogram flatness criterion was set to  $10^{-6}$ , to ensure that the simulation continues until the minimum modification factor is reached. This setting ensures good statistical convergence of the histograms for the macroscopic binding states. The obtained flatness of the overall histogram was always better than 0.025. Macroscopic properties were computed in terms of the intrinsic energies of the binding macrostates (see section A.1 of the Supporting Information).

Probabilities of binding states and conformations for individual sites were computed with the Metropolis MC method.<sup>51</sup> We used 500 MC scans for the equilibration and  $2 \times 10^5$  MC scans

for the production run. The statistical error of all probabilities was below  $10^{-3}$ .

Free energy calculations were performed with the free energy perturbation method<sup>52</sup> in our recently presented generalization.<sup>53</sup> We used staging<sup>54</sup> with two alchemical intermediate states evenly distributed along the transformation coordinate. The Bennett acceptance ratio method was used to minimize the statistical error of the free energy estimates.<sup>55</sup> Each free energy calculation consisted of multiple short simulations. The number of simulations was increased until the statistical error of the free energy estimate was smaller than 0.005 kcal/mol. Each separate simulation consisted of 500 MC scans for equilibration and 2000 to 10 000 MC scans for production. During production, microstate energy difference samples were collected after each MC scan according to the multimove simulation scheme.<sup>19,53</sup>

Events in a molecule can be described by reactions of sites or groups of sites in the molecule. The cooperativity between reactions can be measured with the cooperativity free energy  $G^{\text{coop.}(n)}$ , where the order  $n$  in the superscript denotes the number of reactions between which the cooperativity is measured. A negative cooperativity free energy indicates that the reactions favor each other; i.e., that they are cooperative. A positive cooperativity free energy indicates that the reactions disfavor each other, i.e., that they are anticooperative. If the cooperativity free energy is equal to zero, the reactions do not influence each other. Cooperativity free energies<sup>18,19</sup> can be computed according to the thermodynamic schemes in Figure 2. The cooperativity free energies between a pair and a triplet of reactions are given by

$$G^{\text{coop.}(2)} = G_{(0,0) \rightarrow (1,1)} - (G_{(0,0) \rightarrow (1,0)} + G_{(0,0) \rightarrow (0,1)}) \quad (4)$$

$$G^{\text{coop.}(3)} = G_{(0,0,0) \rightarrow (1,1,1)} - (G_{(0,0,0) \rightarrow (1,0,0)} + G_{(0,0,0) \rightarrow (0,1,0)} + G_{(0,0,0) \rightarrow (0,0,1)}) \quad (5)$$

The reaction free energies occurring in eqs 4 and 5 are defined and indicated in the thermodynamic schemes in Figure 2. Thereby, the direction in which the reaction proceeds is important and determined by defining the initial and final states of the reaction accordingly. A useful property of the pair cooperativity free energy is that it changes its sign but preserves its absolute value, if the direction of one of the reactions is reversed. We wanted to determine to what extent the cooperativity free energy is influenced by sites that are not directly involved in the separate reactions defining the cooperativity free energy. We quantified the influence of these sites with the difference between the cooperativity free energy calculated for the whole system and the cooperativity free energy computed in the absence of other sites. The absence of these sites was mimicked by setting their interaction energies with the sites immediately involved to zero.

### 3. RESULTS AND DISCUSSION

**Coupling of Overall Protonation and Reduction.** We began the characterization of PaAz by studying the coupling of its protonation and reduction from an overall, i.e., macroscopic, viewpoint. Here, macroscopic means that the total numbers of protons and electrons bound to PaAz are considered without regard to individual binding sites. Parts a and b of Figure 3 show the effect of reduction on the macroscopic protonation probabilities of PaAz as a function of the pH value. It can be seen that

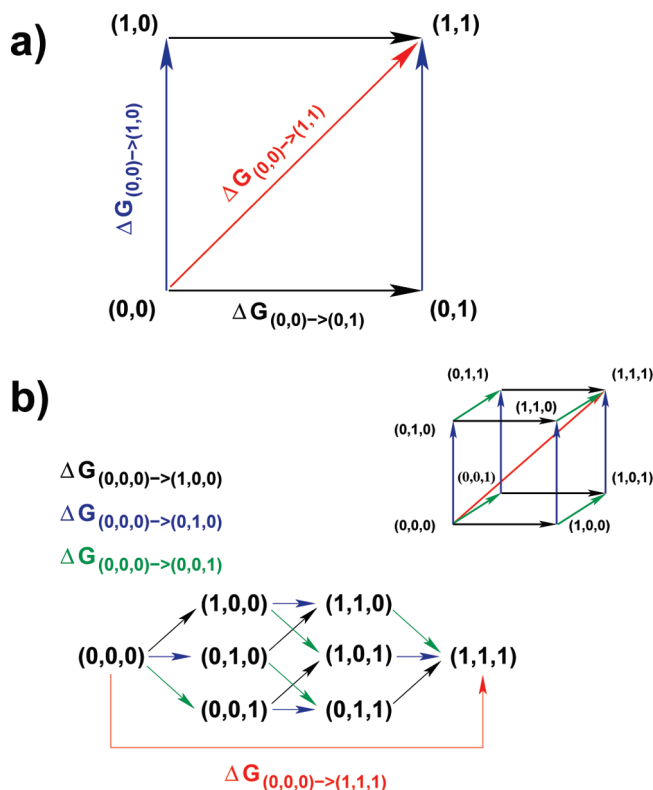
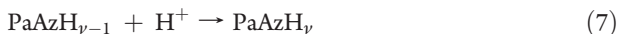


**Figure 2.** Thermodynamic schemes for the calculation of the free energy of cooperativity between (a) a pair and (b) a triplet of reactions. The states and free energy differences that occur in the calculation are indicated. The states of the system are denoted by a pair or a triplet of numbers in braces. The first number stands for the first reaction, the second number for the second reaction, and the third number for the third reaction (in case of the triplet cooperativity). The number 0 indicates the initial state of a reaction, and the number 1 indicates the final state of a reaction.

the greatest effect of reduction occurs in the intermediate range of values between pH 6.0 and 8.0. The average number of protons taken up by PaAz upon reduction is plotted in Figure 3c in dependence on the pH value. It can be seen that the average number of protons taken up is smaller than 1 for the whole range of pH values. The proton uptake reaches a maximum in the intermediate range of pH values in agreement with panels a and b of Figure 3 and experimental findings.<sup>56–58</sup>

The coupling between the protonation and the reduction reactions of PaAz can be quantified with cooperativity free energies. These cooperativity free energies can be interpreted as effective interaction energies between the electron taken up in the reduction reaction and the protons bound in the protonation reaction. Figure 3d shows the cooperativity free energy between the reduction reaction and stepwise protonation reactions of PaAz. The two reactions can be formally written as



where  $v$  indicates the number of protons bound at the final state of the  $v$ th protonation step. From Figure 3d, it can be seen that the cooperativity between the stepwise protonation reactions is highest for the first protonation step. The 19th and 20th

protonation steps are the only other protonation steps with cooperativity free energies that are significantly greater than the thermal energy. The high magnitude of the cooperativity free energy for these protonation steps is mainly based on the involvement of the two protonation steps of His-35 which is in close distance to the copper center. The total effective interaction energy between the electron and the bound protons in reduced PaAz can be quantified with the cooperativity free energy between the reduction reaction and the overall protonation reaction. The reaction equation for the reduction reaction is given by eq 6. The reaction equation for binding  $v$  protons is given by



The total effective interaction energy between the electron and the protons in reduced PaAz is plotted in Figure 3e as a function of the total number of protons bound. In agreement with Figure 3d, it can be seen that about one-third of the interaction is already gained in the first protonation step. Furthermore, it can be observed that the rise in the effective interaction per protonation step is almost constant for the remaining steps except for the 15th to 20th and the last two protonation steps.

**Titration Behavior of Individual Sites.** Following the investigation of the macroscopic binding behavior of PaAz, we studied its behavior from a microscopic viewpoint by analyzing the titration behavior of individual sites. We started with a validation of our computational method by comparing our computed titration curves to available experimental data. Then we performed a detailed analysis of the binding equilibria and conformational equilibria of individual sites using free energy calculations. We concentrate the discussion on the copper center, the peptide flip region, His-35, and His-83, because these sites are involved in the coupling of protonation reduction and conformational change.<sup>12–16</sup> His-35 and His-83 are the only protonatable sites that interact strongly with the copper center and titrate in the physiologically relevant neutral range of pH values.

We correlated the computed titration behavior of important sites with experimentally determined midpoint reduction potentials ( $\epsilon_{1/2}$ ) and  $pK_a$  values ( $pK_{1/2}$ ). The comparison of experimental and theoretical data is summarized in Figure 4. The calculated midpoint reduction potentials of the copper center agree well with the experimental data except for very alkaline pH values where the deviation is larger. Interestingly, more recent voltammetry experiments on PaAz immobilized on electrode surfaces showed a larger decrease in reduction potential at alkaline pH values in agreement with our results.<sup>21,58</sup> We did not use these data for comparison because it is not possible to quantify the influence of the electrode surface on the midpoint potentials.

The overall dependence of the reduction on the pH value of the solution is somewhat overestimated in our calculation, as judged from the steeper slope of the calculated curve of midpoint potentials relative to the experimental data. The overestimation of couplings by continuum electrostatic models originates in most cases from larger conformational arrangements that are not explicitly represented in the model.<sup>27,67</sup> The overestimated coupling can most likely be explained by the absence of explicit backbone flexibility in our model. Such flexibility has been reported for the loop regions of PaAz on the basis of NMR experiments.<sup>16,22</sup> An additional factor within the continuum electrostatic approach that can contribute to the overestimation

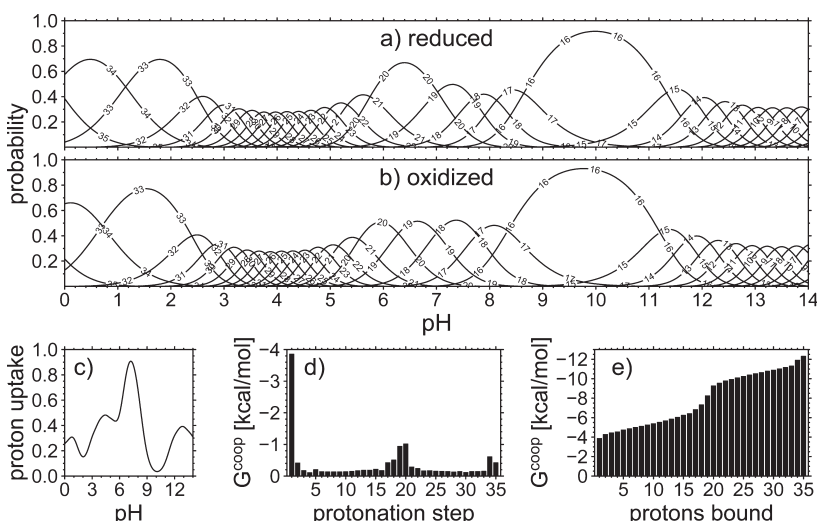


**Figure 3.** Macroscopic binding properties of PaAz. Top: Macroscopic protonation probabilities for (a) reduced and (b) oxidized PaAz as a function of the pH value. The numbers inscribed in the curves indicate the number of protons bound by the respective protonation macrostate. Bottom: (c) Average number of protons taken up upon reduction as a function of the pH value. (d) Macroscopic cooperativity free energy between protonation and reduction for each macroscopic protonation step (gain of effective interaction energy between the protons and the electron in the macroscopic binding reaction). (e) Total macroscopic cooperativity free energy as a function of the number of bound protons (effective interaction energy between the protons and the electron).

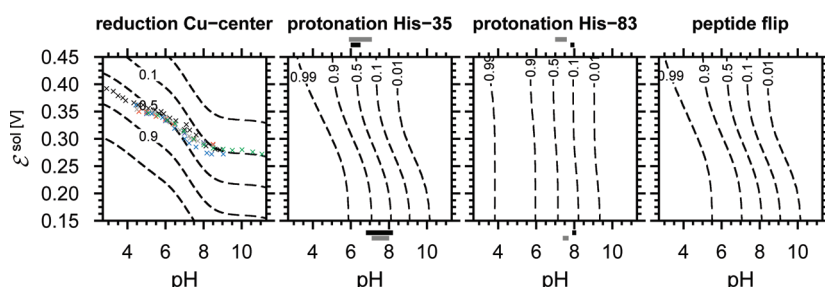


**Figure 4.** Validation of our model by comparison of computed titration curves with experimental midpoint reduction potentials  $\varepsilon_{1/2}$  and  $pK_{1/2}$  values. The reduction probability of the copper center, the protonation probabilities of His-35 and His83, and the occupation probability of the low-pH form of the peptide flip region are plotted as functions of the pH value and reduction potential of the solution  $\varepsilon^{\text{sol}}$ . The probabilities are indicated by labeled isocontours. Experimental  $\varepsilon_{1/2}$  and  $pK_{1/2}$  values should ideally coincide with the regions where the calculated reduction and protonation probabilities adopt a value of 0.5. Experimental midpoint reduction potentials are plotted in the leftmost panel as colored crosses. The corresponding data are taken from the following references: black, 59; gray, 15; red, 60; green, 14; dark blue, 61 and 62; light blue, 63. The ranges of experimentally determined  $pK_{1/2}$  values from direct measurements with NMR are shown as black bars.<sup>14,16,64–66</sup> The ranges of  $pK_{1/2}$  values that are indirectly determined from fits to kinetic and/or voltammetry experiments are shown as gray bars.<sup>20,21,56,58</sup> The bars above the plots (high  $\varepsilon^{\text{sol}}$ ) correspond to oxidized PaAz, whereas the bars below the plots (low  $\varepsilon^{\text{sol}}$ ) correspond to reduced PaAz. Titration curves of all residues of PaAz and pictures of PaAz indicating their spatial positions can be found in section A.2 of the Supporting Information.

of interaction energies lies in the necessity to assume the presence of multiple conformers of the sites in the definition of the dielectric boundaries,<sup>48</sup> where there is no formally exact and theoretically satisfactory method to correct for this effect. Empirical corrections proposed in the literature<sup>48</sup> were not employed in this study, but the effect was minimized by considering only surface-exposed, mobile residues as flexible and by removing energetically unfavorable side chain rotamers from the calculations (see Methods).

The titration curves of the His-35 and His-83 are depicted in the two central plots of Figure 4. In the following, protonation of a histidine side chain refers to the binding of a proton to one of the singly protonated forms of the histidine side chain to form the doubly protonated imidazolium form. For both histidine residues, the fully deprotonated imidazolate form is included in the

calculation but does not have a significant occupation probability in the studied pH range. The singly protonated tautomers that are populated by His-35 and His-83 in our simulations are consistent with experimental findings. The population of the  $N_{\delta}$  tautomer by the deprotonated His-83 and the  $N_e$  tautomer by the deprotonated His-35 comply with results from NMR experiments.<sup>65</sup> The population of the  $N_e$  tautomer by the deprotonated His-35 is also clearly evident from the available structural information at a pH value of 9.0<sup>12</sup> (see Figure 1b). The  $pK_{1/2}$  values of His-35 and His-83 are consistent with direct NMR measurements<sup>14,64–66</sup> and indirect fits to kinetic<sup>20,56</sup> and voltammetry data.<sup>21,58</sup> Even  $pK_{1/2}$  values that are measured directly with NMR are afflicted with a typical methodological uncertainty of  $\approx 1$  pH unit.<sup>56,68</sup> In some individual cases the uncertainty can reach higher values.<sup>56,68</sup> This uncertainty can

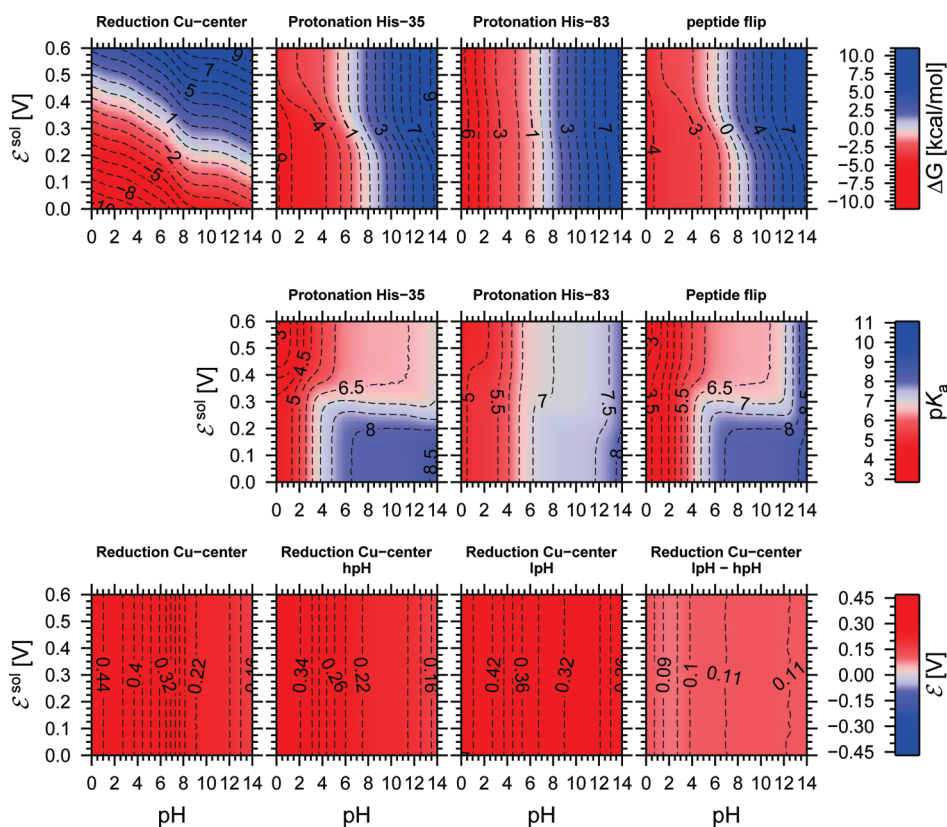


**Figure 5.** Reaction free energies for reactions that are involved in the coupling of protonation, reduction and conformational change in PaAz. Top row: The reaction free energies are plotted as functions of the pH value and the reduction potential of the solution. The reaction free energy is color coded (see color bar). Contours are plotted in constant intervals of 1.0 kcal/mol. Contour values are given in kilocalories per mole. Middle row: The reaction free energies are replotted from the top row as thermodynamically defined Henderson–Hasselbalch  $pK_a$  values calculated from  $pK_a = \text{pH} - \beta\Delta G^{\text{prot}}/(\ln 10)$ .<sup>70,71</sup> The tight coupling between the protonation of His-35 and the peptide flip leads to an apparent  $pK_a$  value of the peptide flip that is over wide ranges of solution pH and reduction potential very similar to the  $pK_a$  value for protonating His-35. The  $pK_a$  value is color coded (see color bar). Contours are plotted in constant intervals of 0.5 pH units. Contour values are given in pH units. Bottom row: The reduction free energy of the copper center is plotted as thermodynamically defined Nernst reduction potential calculated from  $\mathcal{E} = \mathcal{E}^{\text{sol}} - \Delta G^{\text{red}}/F$ .<sup>70</sup> The leftmost plot shows the reduction potential for the unconstrained system. The two central plots show the reduction potential for PaAz constrained to either the hpH or the lpH form. The rightmost plot shows the difference between the reduction potentials of PaAz in the lpH and hpH forms. Contours are plotted in constant intervals of 10 mV for the rightmost plot and in constant intervals of 20 mV for the other plots. Contour values are given in volts. The corresponding plots for other sites in PaAz can be found in section A.3 of the Supporting Information.

originate from interactions of the chosen reporter nucleus with other sites in the vicinity of the monitored site.<sup>68</sup> The indirectly determined experimental  $pK_{1/2}$  values slightly deviate from the NMR measured values. The overall agreement of our calculated  $pK_{1/2}$  values with the NMR data is better than with the indirectly determined data. The indirectly determined values rely on a fit of experimental data to mathematical models that assume the coupling of the reduction to one (His-35) or two (His-35 and His-83) protonatable sites. We show below that there are more than two protonatable sites that contribute to the coupling of protonation and reduction in PaAz. Thus, the NMR data are to be preferred as reference over the indirectly determined data. In agreement with both kinds of experiment, the protonation probability of His-35 is much more dependent on the reduction of the copper center than the protonation of His-83.

The rightmost plot of Figure 4 shows the occupation probability of the low-pH form of the peptide flip region as a function of the pH value and the reduction potential of the solution. We found that the conformational change of the peptide flip region depends on both parameters and thus on the protonation and reduction of PaAz. This finding is consistent with experimental

findings.<sup>12,16,69</sup> The titration curve of the peptide flip region at low reduction potentials has a midpoint at a value of about pH 8.0. This value is consistent with a value between pH 5.5 and 9.0 implied by the structural data<sup>12</sup> (see Figure 1). Our value is slightly higher than the value of 7.0, which can be deduced from the experimental equilibrium constant of  $\approx 1$  for reduced PaAz at pH 7.0 inferred from kinetic experiments.<sup>69</sup> Given the uncertainty in the experimental data, and the simplicity of the continuum electrostatic model, the agreement of our calculations with experiment is satisfactory.

The top row of Figure 5 shows plots of the reaction free energies corresponding to the titration curves in Figure 4. The reduction free energy of the copper center, the protonation free energies of His-35 and His-83, and the conformational free energy of the peptide flip show a complex dependency on the pH value and the reduction potential of the solution. In support of our previous findings,<sup>70–72</sup> it can be seen that the titration behavior of sites in a protein differs markedly from that of isolated model compounds in solution. In effect, the thermodynamics of protonation and reduction of sites in a protein cannot be described by ascribing a single  $pK_a$  value<sup>71,72</sup> or reduction

potential to these sites.<sup>70</sup> The coupled titration behavior of these sites is caused by the electrostatic interactions between sites in a protein.<sup>72</sup> These interactions can act over considerable distances especially if the interacting sites are charged. The coupling between the sites is analyzed in detail as follows.

The close similarity of the shapes of the titration and free energy curves for the protonation of His-35 and the peptide flip points to a tight coupling between the two reactions. This finding is in agreement with experimental findings.<sup>16,21</sup> The favorable effective interaction is caused by the complementary hydrogen-bonding properties of the peptide flip region and the side chain of His-35, where each of the bonding partners can either be a hydrogen bond acceptor or donor. The strong favorable microscopic interactions between pairs formed from a hydrogen bond donor and a hydrogen bond acceptor and the strong unfavorable microscopic interactions between pairs of two hydrogen bond donors or two hydrogen bond acceptors lead to the strongly coupled titration behavior of the sites. This coupling is so strong that PaAz occurs almost exclusively in either a high-pH form or a low-pH form. In the high-pH form (hpH), His-35 is deprotonated and the peptide flip region is in the high-pH conformation seen in PDB 5AZU<sup>12</sup> (see Figure 1b). In the low-pH form (lpH), His-35 is protonated and the peptide flip region is in the low-pH conformation seen in PDB 4AZU<sup>12</sup> (see Figure 1c). See Figure S6 of the Supporting Information for plots of the occupation probabilities of the two forms and of the residual probability.

The reduction probability of the copper center in the neutral pH range is strongly dependent on the pH value of the solution. Similarly, the protonation probabilities of His-35 and His-83 are dependent on the reduction potential of the solution in the neutral pH range. The stronger dependency in the case of His-35 can be rationalized from the strong electrostatic repulsion between the oxidized copper center and the protonated side chain of the nearby His-35. The much weaker dependence in the case of His-83 can be rationalized from its more remote location and consequently weaker electrostatic interaction with the copper center.

The protonation free energy can be expressed and plotted in terms of a thermodynamically defined Henderson–Hasselbalch  $pK_a$  value<sup>70,71</sup> (see the middle row of Figure 5). This representation of the protonation free energy makes especially clear that both sites exhibit a  $pK_a$  value that depends on both the pH value and the reduction potential of the solution. Also the much stronger dependence of the protonation of His-35 relative to the protonation of His-83 on the reduction potential of the solution is especially clearly seen in this representation of the protonation free energy.

Analogously, the reduction free energy of the copper center can be written in terms of a thermodynamically defined Nernst reduction potential<sup>70</sup> (see the bottom row of Figure 5). It can be seen that the reduction potential of the copper center does not depend on the reduction potential of the solution, as can be expected in the absence of other redox-active sites.<sup>70</sup> Furthermore, it can be seen that the reduction potential of the copper center depends on the pH value of the solution. This dependency results from the interaction with the surrounding protonatable sites.

**Coupling between Protonation, Reduction, and Conformational Change on the Level of Individual Sites.** Following the investigation of the titration behavior of the individual sites, we analyzed the coupling between their reactions. Cooperativity free energies between reactions can be used to analyze their

coupling and provide a quantitative measure of the coupling strength.<sup>18,19</sup> The cooperativity free energy has a straightforward interpretation as effective relative interaction energy between the reacting sites.<sup>18,19</sup> The cooperativity free energy between a pair of events is conceptually identical to the effective interaction energy measured in a double mutant cycle experiment.<sup>73,74</sup> For our analysis, we considered all reactions of individual sites in PaAz that could be involved in the coupling between protonation, reduction, and conformational change. We considered the protonation reactions of all residues, the reduction reaction of the copper center, and the conformational change of the peptide flip region from the high-pH form to the low-pH form. The cooperativity free energies between all pairs of considered reactions in PaAz are shown in Figure 6a for a pH value of 7.0.

Not surprisingly, it can be seen that there is significant anticoperativity for most pairs of protonation reactions of sites that are in close distance, due to the electrostatic repulsion between the proton charges. A decrease of the effective repulsion between some pairs of protonation reactions can arise from the release of protons from nearby third sites.<sup>19,75,76</sup> This effect can even lead to an apparent attractive interaction between protons bound to pairs of interacting protonatable sites as in the case of His-35 and Asp-11 or Lys-74 and Arg-79. Also the favorable effective interaction between the protonation of almost all sites and the reduction of the copper center could be expected on the basis of the attractive electrostatic interaction between the complementary charges of the ligands. It can be seen that apart from His-35 and His-83 many other residues contribute to the cooperativity of protonation and reduction. The main contribution comes, however, from His-35, which is consistent with its location close to the copper center (see Figure 1) and earlier work.<sup>56,57,77</sup> The fit of experimental data to mathematical models that assume only one or two protonatable sites which are coupled to the reduction reaction implicitly include the contributions of all the other sites. Thus,  $pK_a$  values of the histidine residues inferred from such fits necessarily deviate somewhat from their true  $pK_a$  values. This finding explains the disagreement between  $pK_{1/2}$  values from direct measurements and indirect fits and why our calculated  $pK_{1/2}$  values agree better with direct NMR measurements.

The influence of third sites on the cooperativity free energy can be estimated by taking the difference between the cooperativity free energies calculated for the whole system and calculated in the absence of interactions with third sites (see Methods). The pairwise cooperativities between the isolated sites are equivalent to the relative microscopic interaction energies used in traditional two-state binding models (see, e.g., refs 45 and 32). The influence of the other sites on the cooperativity free energy can be seen to dampen the magnitude of the cooperativity free energies relative to the cooperativity free energy between the isolated sites in most, but not all, cases. Especially the cooperativity free energy between the peptide flip and the reduction of the copper center is increased by the surrounding sites. This effect will be analyzed in more detail below. The cooperativity free energies of the reduction of the copper center and the protonation of all protonatable sites is decreased by the influence of the surrounding sites. This dampening of the effective coupling between the reducible site and the protonatable sites contributes to the relatively low proton uptake upon reduction (see Figure 3c) and the overall pH dependence of the reduction potential of PaAz.

From Figure 6a, it can be seen that the coupling between protonation, reduction, and conformational change in PaAz is

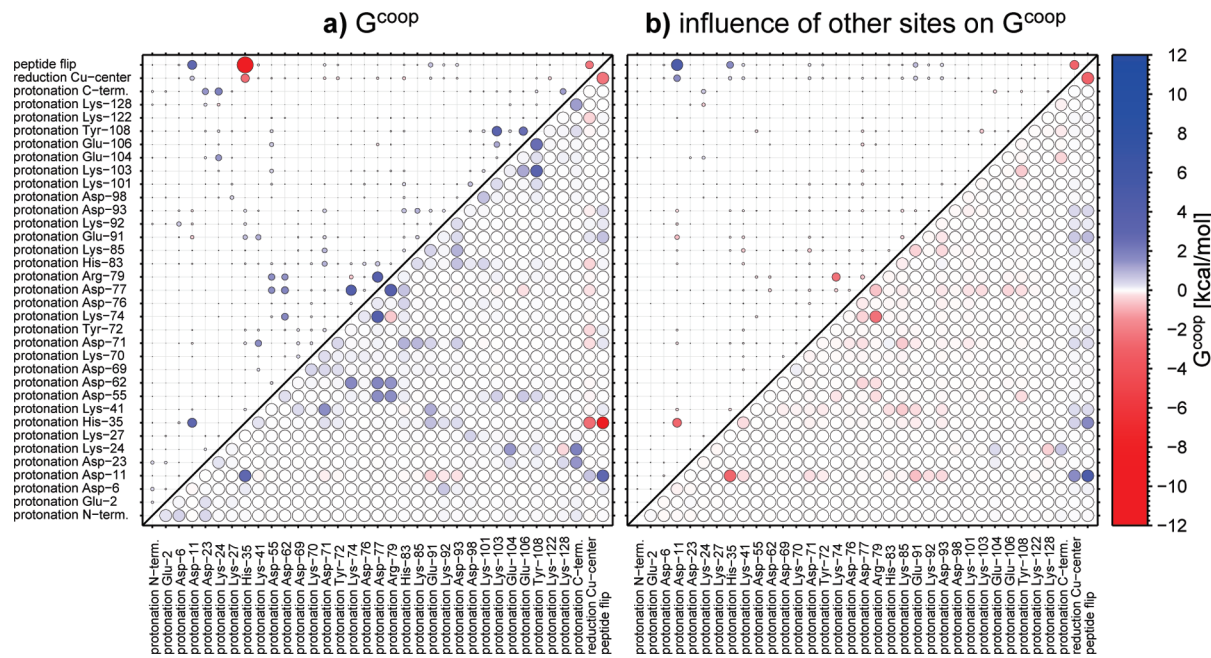


**Figure 6.** Pairwise cooperativity free energies between reactions of sites in PaAz at pH 7.0 and  $\epsilon^{sol} = 0$ . The reactions are indicated by the labels on the plot axes. The symbols are colored according to the magnitude of the cooperativity free energy (see color bar). For easier spotting of cooperativities with a large magnitude, the symbols in the upper left triangles are scaled such that their area is proportional to the magnitude of the cooperativity free energy. See Figures S10–S12 of the Supporting Information for numeric values. (a) Cooperativity free energy for the whole system. (b) Difference between the cooperativity free energies for the whole system and for the isolated sites (all interactions with other sites set to zero) as a measure of the influence of surrounding sites on the cooperativity free energy.

almost entirely contributed by only three sites. These sites are the copper center, His-35, and the peptide flip region. In the following, we concentrate on the cooperativity between the reactions of these sites for a more detailed analysis.

The cooperativity free energies between all possible pairs and the triplet formed from the reduction of the copper center, the protonation of His-35, and the peptide flip are plotted as functions of the pH value and the reduction potential of the solution in Figure 7. It can be seen that the pair cooperativity free energies do not depend strongly on the pH value and the reduction potential of the solution, but are instead nearly constant over wide regions of the parameter space. A similar behavior was also found for the other pair cooperativity free energies in Figure 6 (see Figure S13 of the Supporting Information).

The similarity of the titration behavior of His-35 and the peptide flip region already suggested a strong coupling between the protonation of His-35 and the conformational change of the peptide flip region (see Figure 4 and Figure 5). This suggestion is corroborated by the high magnitude of the cooperativity free energy between the two reactions over the whole range of ligand chemical potentials investigated (see Figure 7). Above, we also demonstrated a strongly pH-dependent titration behavior of the copper center, which points to the presence of at least one strongly interacting protonatable site. The cooperativity free energy between the protonation of His-35 and the reduction of the copper center adopts a nearly constant value of  $-2.3 \text{ kcal/mol}$  for pH values between 4.0 and 14.0 (see Figure 7). This effective interaction energy is responsible for the upshift of about 100 mV in the reduction potential of the copper center upon conversion from the high-pH to the low-pH form (see Figure 5, bottom right).

As already seen from Figure 6, the positive cooperativity between the reduction of the copper center and the peptide flip is not caused by the direct microscopic interaction between the copper center and the peptide flip region. Taken separately, the electrostatic interaction between the two sites would even lead to weak anticooperativity between their reactions. The basis for the positive cooperativity between the two reactions are mediating, mainly electrostatic interactions of His-35 with the copper center and the peptide flip region. This can be demonstrated by computing the cooperativity free energy between the reduction of the copper center and a concerted reaction consisting of the protonation of His-35 and the peptide flip. We showed above that the coupling between these two reactions is so tight that PaAz is essentially always found in one of two forms under equilibrium conditions. The label  $hpH \rightarrow lpH$  above the plots in the upper right plots of Figure 7 indicates this concerted reaction that converts PaAz from the high-pH form to the low-pH form. It can be seen that there is nearly no influence of other sites on the cooperativity free energy between the reduction of the copper center and the concerted reaction. This finding proves that the positive cooperativity between the reduction of the copper center and the peptide flip is mediated by electrostatic interactions of both sites with His-35. This arrangement can be symbolized by the linear interaction scheme BCC–His-35–PEP, where BCC stands for blue copper center and PEP for the peptide flip region and a long hyphen symbolizes a strong coupling. That is, the interaction of the peptide flip region with His-35 is relayed to the copper center. Likewise, the interaction of the copper center with His-35 is relayed to the peptide flip region.

The bottom half of Figure 7 shows the triplet cooperativity free energy between the reduction of the copper center, the protonation of His-35, and the peptide flip in comparison to the

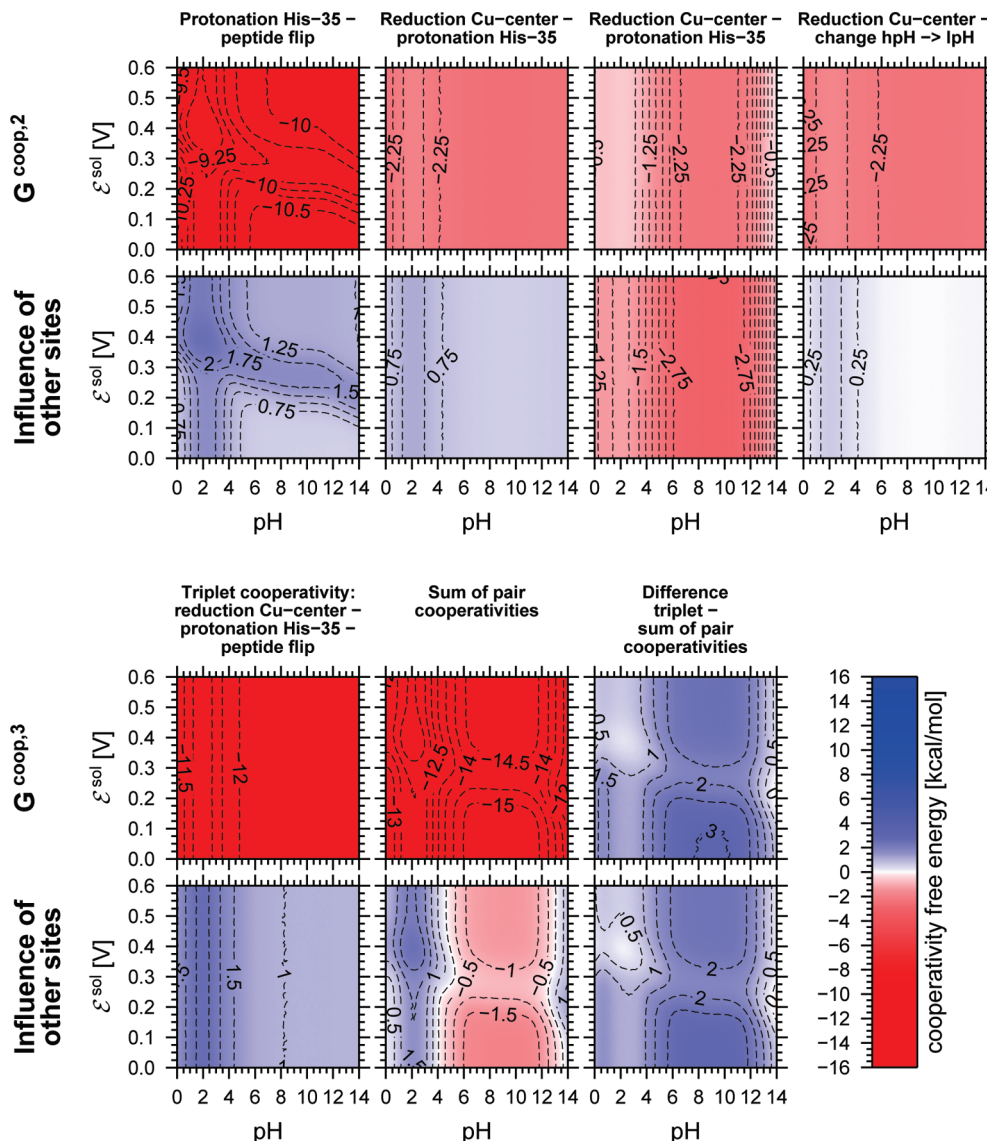


**Figure 7.** Cooperativity free energies between reactions involved in the coupling of protonation, reduction and conformational change in PaAz plotted as functions of the pH value and the reduction potential of the solution. Top: Pair cooperativity free energies between the reactions that are indicated above the curves. Bottom: The triplet cooperativity free energy between the reactions considered in the first three columns of the above block in comparison to the sum of the corresponding pair cooperativity free energies. The upper rows of the bottom and top blocks show the cooperativity free energy calculated for the whole system. The plots in the lower rows shows the influence of the other sites on the cooperativity free energy (see Methods). The cooperativity free energy is color coded (see color bar). The upper and lower blocks are contoured in constant intervals of 0.25 and 0.5 kcal/mol, respectively. Contour values are given in kilocalories per mole. The corresponding plots for other sites in PaAz can be found in section A.4 of the Supporting Information.

sum of the corresponding pair cooperativity free energies. It can be seen that the triplet cooperativity free energy is nearly constant for the greatest part of the chemical potential space, except for a region of low variability in the acidic range of pH values ( $\text{pH} < 5$ ). Furthermore, the triplet cooperativity free energy is not equal to the sum of the pair cooperativity free energies but smaller in magnitude. Such a nonadditive behavior was also found in other systems.<sup>18</sup> Thus, the statistical mechanics of a multisite system can give rise to apparent many-body interactions even if the underlying microscopic energy function contains only pairwise interaction energies.<sup>18</sup> Comparison of the plots on the bottom right of Figure 7 shows that the deviation is dominated by the contributions of the surrounding sites. Thus, the reduced magnitude of

the triplet cooperativity is caused by the relaxation of degrees of freedom of other sites than those directly involved. This finding highlights the importance of using a detailed model that accounts for all protonatable sites, even though the individual contributions of most sites are small.

**Implications of Our Findings for the Physiological Role and Therapeutic Applications of PaAz.** The coupling of protonation reduction and conformational change in PaAz could be important for the physiological role of PaAz and for its role as a therapeutic agent. The physiological electron-transfer partners of PaAz are not known with certainty. Therefore, our discussion has to consider all possible factors that are known to affect electron-transfer reactions.

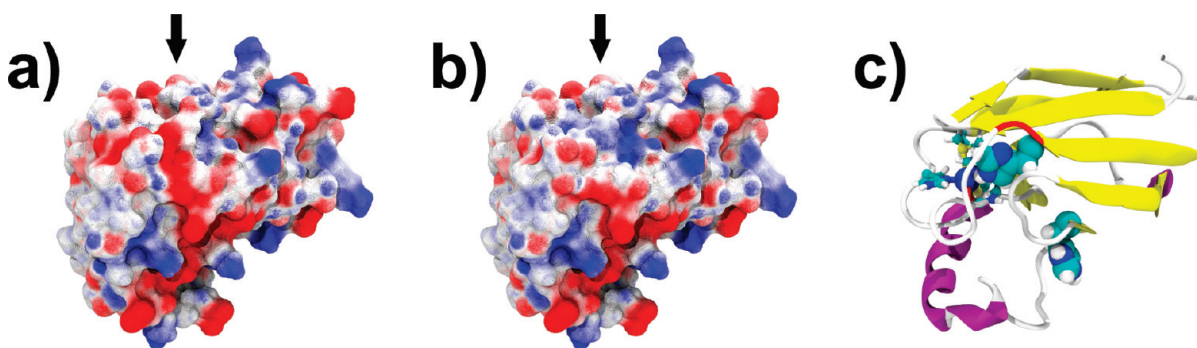


**Figure 8.** Electrostatic potential on the solvent accessible surface of reduced PaAz in (a) the high-pH form and (b) the low-pH form at pH = 7.0. The arrows at the plots indicate a region of variable electrostatic potential at the right rim of the hydrophobic patch above the peptide flip region. This region is termed His-35 patch and was suspected earlier to be involved in the mediation of ET. The color scale for the electrostatic potential reaches from red at  $-77\text{ mV}$  to blue at  $+77\text{ mV}$  ( $\pm 3k_{\text{B}}T/e^{\circ}$ ). The structures of PaAz were constructed by setting all sites to their most highly populated instances within the respective state. There are no significant conformational differences between the states apart from those in the peptide flip region. The electrostatic potentials and solvent accessible surfaces were computed with our in-house version<sup>25</sup> of the MEAD package.<sup>26,27</sup> (c) Structure of PaAz in the same orientation as in panels a and b for orientation. The backbone of Pro-36 and Gly-37 between which the peptide flip occurs is colored red. His-35, His-83, and the copper center are highlighted (cf. Figure 1). The figure was prepared with VMD<sup>23</sup> and Tachyon.<sup>24</sup> See Figure S15 of the Supporting Information for alternative views and equivalent plots for oxidized PaAz.

Electron-transfer reactions between proteins consist of several stages. The electron-transfer partners approach each other in a structurally heterogeneous encounter complex, followed by the formation of a structurally more defined productive complex.<sup>78</sup> Such a two-step binding scheme is believed to apply to all protein–protein binding reactions.<sup>78</sup> The formation of the productive complex can also involve rearrangements in the internal conformation of the binding partners.<sup>79,80</sup> ET reactions whose rate is affected by the steps that precede the actual electron-transfer step are termed coupled or gated.<sup>80</sup> Each of the separate steps can influence the rate for the overall electron-transfer reaction. In contrast, the thermodynamics of the electron-transfer reaction is solely determined by the difference in the reduction potentials of the electron-transfer partners.

We found that the conversion of PaAz from the high-pH form to the low-pH form leads to an increase in its reduction potential of about 100 mV (see Figure 5). This increase in reduction potential has been suggested before as a potential way of down-regulating the electron-transfer activity of PaAz if the pH value in the periplasm becomes too low.<sup>16,77</sup> The change in reduction potential can affect the rate of the actual electron-transfer step and the overall thermodynamics of an electron-transfer reaction. Furthermore, this conversion results in a marked change of the electrostatic potential at the surface of PaAz within the so-called His-35 patch<sup>56,77,81</sup> above His-35 and the peptide flip region (see Figure 8). The negative electrostatic potential of this region seen in the high-pH form is neutralized in the low-pH form. The His-35 patch is located in close distance to the hydrophobic patch, which is known to be the site of direct interaction in electron-transfer reactions of PaAz.<sup>13,82,83</sup> Thus, the change in the electrostatic surface potential could affect the thermodynamics and the kinetics of the binding steps that precede the electron transfer. The importance of electrostatic interactions in electron-transfer reactions of PaAz has been demonstrated experimentally.<sup>84</sup> The hydrophobic patch is most likely also involved in interactions of PaAz with the mammalian tumor suppressor p53 that takes place during the induction of apoptosis by PaAz.<sup>9,85</sup> Thus, the change in the electrostatic potential of PaAz caused by the conversion could influence its interaction with binding partners within its roles as electron carrier and as therapeutic agent.

A similar effect was proposed for the electron-transfer complex of ferredoxin NADP-reductase (FNR) and ferredoxin.<sup>86</sup> In this case, the deprotonation of a glutamate residue close to the redox center of FNR might induce the release of ferredoxin from the complex during the catalytic cycle of FNR.

Instead of a change in the pH value, also electrostatic interaction of PaAz with a binding partner could induce the conversion between the high-pH and low-pH forms. The cooperativity of this conversion with the reduction of the copper center would in effect also shift the reduction potential of PaAz. A possible influence of the electron-transfer partner on the conformational equilibrium of PaAz has been noted before by Jeuken et al. for the case of a metal electrode in voltammetry.<sup>21</sup> A similar situation has been found for the electron-transfer reaction between amicyanin and methylamine dehydrogenase.<sup>87</sup> The presence of methylamine dehydrogenase in the electron-transfer complex prevents the dissociation and protonation of one of the histidine ligands of the copper center of amicyanin. In effect, the reduction potential of the copper center of amicyanin is decreased and the electron transfer from amicyanin to methylamine dehydrogenase becomes more favorable.

If the conversion between the high-pH and low-pH forms has a regulatory function, another aspect of this conversion could be functionally important. Namely, the kinetics of the conversion is very slow.<sup>16,65</sup> Experimentally determined rates for the conversion range from 0.23 to 45 s<sup>-1</sup>.<sup>16,21</sup> In effect, a regulatory signal transferred to PaAz by means of this conversion would decay very slowly on a molecular time scale.

The physiological function of PaAz in *P. aeruginosa* and the identity of physiological redox partners are not yet clearly established. Initially, PaAz was believed to function as electron carrier in respiratory denitrification.<sup>1</sup> In this pathway, *P. aeruginosa* uses nitrite and other intermediates of the denitrification pathway as terminal electron acceptors under anaerobic conditions. PaAz was believed to function as electron donor to cytochrome *cd*<sub>1</sub> nitrite reductase.<sup>1,88,89</sup> The gene for azurin was, however, later found not to be essential for denitrification<sup>3</sup> and not located close to other denitrification genes in the genome of *P. aeruginosa*.<sup>90</sup> Instead, two soluble cytochromes *c* from the nitrite reductase gene cluster were found also to be able to donate electrons to nitrite reductase at similar rates.<sup>91</sup> These cytochromes *c* are

cytochrome  $c_{551}$  (NirM) and NirC. Cytochrome  $c_{551}$  has been reported to be a more efficient electron donor to nitrite reductase than PaAz.<sup>89,92</sup> Also possible roles of PaAz as obligatory electron donor to aromatic amine dehydrogenase or ethanol dehydrogenase have been ruled out.<sup>3</sup> PaAz has also been reported to accept electrons from cytochrome  $bc_1$  if the bacterium utilizes succinate as electron donor, where again cytochrome  $c_{551}$  can fulfill the same function.<sup>4</sup> PaAz expression was found to be induced under oxidative stress conditions and to contribute to the oxidative stress resistance.<sup>3</sup>

The finding that PaAz does not have an essential role as electron carrier in denitrification<sup>3</sup> does not necessarily mean that it never fulfills this function *in vivo*. The presence of multiple, seemingly redundant electron carriers that are able to fulfill the same function is not unprecedented. An example is found in photosynthesis of cyanobacteria. Both the roles of the electron donor and of the electron acceptor of photosystem I can be fulfilled by two different proteins in these bacteria.<sup>93–96</sup> The electron donor plastocyanin which utilizes a type-1 copper center is replaceable by cytochrome  $c_6$  under copper deficiency.<sup>96,97</sup> The electron acceptor ferredoxin which utilizes an iron–sulfur center can be replaced by flavodoxin under iron deficiency.<sup>96,98</sup> One might ask, if the redundancy of PaAz and the cytochromes *c* as electron donors to the nitrite reductase of *P. aeruginosa* does also confer resistance against copper or iron deficiency.

It seems also conceivable, that the physiological function of PaAz is not that of an electron carrier between a single electron donor and a single electron acceptor. *P. aeruginosa* possesses versatile metabolic capabilities<sup>99</sup> and a branched respiratory system with several alternative terminal oxidases.<sup>4,100,101</sup> If PaAz does not possess a strictly essential role, it seems conceivable that it fulfills a regulatory function. The ability of PaAz to interact with different redox partners could enable it to distribute electrons between different branches of the respiratory system. Such a role could also explain how PaAz contributes to the resistance of the bacterium against redox stress.<sup>3</sup> Vijgenboom and co-workers pointed out that an increased amount of PaAz could help to avoid toxic levels of nitric oxide which could accumulate in the cell if there is an excess of reducing substrates for nitrite reductase.<sup>3</sup>

In light of our findings, one might also ask whether such a function for PaAz would be modulated by the pH value of the solution and/or the ready availability of electron acceptors for PaAz. Instead of completely shutting down or slowing the electron flow between a single electron donor and a single electron acceptor, a different role could be proposed for the pH-dependent transition of PaAz between the high-pH and low-pH forms. The alteration of the electrostatic surface potential of PaAz that accompanies the transition could change the relative affinity of PaAz for different redox partners. This mechanism could form the basis for the proposed balancing of the electron flow through different branches of the respiratory system. Pseudospecific interaction surfaces of electron-transfer proteins have been proposed before to allow for electron transfer with different reaction partners in dependence on external conditions.<sup>102</sup> Besides by a decrease in pH, the transition between the high-pH form and the low-pH form is also favored by the reduction of the copper center (see above). Since this transition is very slow,<sup>16,21</sup> the following scenario seems conceivable. If electron acceptors for PaAz are readily available, the transition does not happen because PaAz is quickly reoxidized. If, on the other hand, the amount of electron donors for PaAz becomes large and electron acceptors are not readily available, PaAz might

undergo the transition from the high-pH form to the low-pH form. The accompanying increase in the reduction potential and the altered electrostatic surface potential might then redirect PaAz toward alternative electron acceptors. The resulting redirection of the electron flow toward alternative electron sinks could prevent harmful effects of excess reducing power such as those described by Vijgenboom et al.<sup>3</sup>

## 4. CONCLUSIONS AND OUTLOOK

We investigated the cooperativity between protonation, reduction, and conformational change in PaAz and discussed possible implications for the function of PaAz. The hydrogen bonding between His-35 and the peptide flip region on the one hand and the electrostatic interaction of His-35 and the copper center on the other hand lead to an effective coupling between protonation, reduction, and conformational change. Furthermore, we found that the conversion between the high-pH form and the low-pH form leads to a marked alteration of the electrostatic potential at the surface of PaAz. This alteration might affect the interaction of PaAz with its binding partners and could thus be relevant for the roles of PaAz as electron carrier and as therapeutic agent. In turn, interactions of PaAz with binding partners can affect the reduction potential of PaAz by shifting the equilibrium between its high-pH and low-pH forms.

We also used PaAz as a model system to demonstrate that structure-based calculations of cooperativity free energies are useful in detecting and quantifying cooperativity between events in biomolecules. There is a large body of experimental literature on PaAz, which could be used to verify our results. The calculation of cooperativity free energies permitted us to add a quantitative description of the coupling between these events and to reveal some yet unknown details. We believe that calculations of cooperativity free energies can provide valuable contributions for the deciphering of mechanistic details in more complex systems that are less accessible to experiment. In principle, cooperativity free energy calculations have an experimental pendant in double and triple mutant cycle experiments.<sup>73,74</sup> Such experiments are, however, not applicable in the case of protein cofactors or if the mutation induces larger structural changes in the protein. In addition, it might be impractical to carry out screening experiments for many different sites that could be mechanistically important. The identity of mechanistically important sites in complex bioenergetic systems is often far from obvious. Obvious candidates for an application of cooperativity free energy calculations are complex bioenergetic systems in which mechanistic details are still debated. Such systems are bacterial reaction centers,<sup>103</sup> photosystems I and II,<sup>93,94,104</sup> cytochrome *c* oxidase,<sup>105,106</sup> and the cytochrome  $bc_1$  and  $b_f$  complexes.<sup>107–109</sup>

## ■ ASSOCIATED CONTENT

**S Supporting Information.** Additional plots and figures referenced in the text and atomic partial charges and intrinsic energies of model compounds used in this work. This material is available free of charge via the Internet at <http://pubs.acs.org>.

## ■ AUTHOR INFORMATION

### Corresponding Author

\*E-mail: thomas.ullmann@uni-bayreuth.de (R.T.U.); matthias.ullmann@uni-bayreuth.de (G.M.U.).

## ACKNOWLEDGMENT

We gratefully acknowledge useful discussions with Verónica I. Dumit. This work was supported by the Deutsche Forschungsgemeinschaft through Grant DFG UL 174/8-1.

## REFERENCES

- (1) (a) Horio, T. *J. Biochem.* **1958**, *45*, 195–205. (b) Horio, T. *J. Biochem.* **1958**, *45*, 267–279.
- (2) Adman, E. T. *Curr. Opin. Struct. Biol.* **1991**, *1*, 895–904.
- (3) Vlijgenboom, E.; Busch, J. E.; Canters, G. W. *Microbiology* **1997**, *143*, 2853–2863.
- (4) Hasegawa, N.; Arai, H.; Igarashi, Y. *Biosci. Biotechnol. Biochem.* **2003**, *67*, 121–126.
- (5) (a) Schobert, M.; Jahn, D. *Int. J. Med. Microbiol.* **2010**, *300*, 549–556. Cystic Fibrosis: (b) Schobert, M.; Tielen, P. *Future Microbiol.* **2010**, *5*, 603–621.
- (6) Yoon, S. S. *J. Bacteriol. Virol.* **2010**, *40*, 59–66.
- (7) Yamada, T.; Hiraoka, Y.; Gupta, T. K. D.; Chakrabarty, A. M. *Cell Cycle* **2004**, *3*, 752–755.
- (8) Chaudhari, A.; Fialho, A. M.; Ratner, D.; Gupta, P.; Hong, C. S.; Kahali, S.; Yamada, T.; Haldar, K.; Murphy, S.; Cho, W.; et al. *Cell Cycle* **2006**, *5*, 1642–1648.
- (9) Goto, M.; Yamada, T.; Kimbara, K.; Horner, J.; Newcomb, M.; Gupta, T. K. D.; Chakrabarty, A. M. *Mol. Microbiol.* **2003**, *47*, 549–559.
- (10) Apiyo, D.; Wittung-Stafshede, P. *Biochem. Biophys. Res. Commun.* **2005**, *332*, 965–968.
- (11) Yamada, T.; Fialho, A. M.; Punj, V.; Bratescu, L.; Gupta, T. K. D.; Chakrabarty, A. M. *Cell. Microbiol.* **2005**, *7*, 1418–1431.
- (12) (a) Nar, H.; Messerschmidt, A.; Huber, R.; van de Kamp, M.; Canters, G. W. *J. Mol. Biol.* **1991**, *221*, 765–772. (b) Nar, H. Röntgenkristallographische Strukturaufklärung von Azurin aus *Pseudomonas aeruginosa*, Ph.D. thesis, Technical University of Munich, Munich, Germany, 1992.
- (13) van de Kamp, M.; Floris, R.; Hali, F. C.; Canters, G. W. *Eur. J. Biochem.* **1990**, *194*, 109–118.
- (14) van de Kamp, M.; Canters, G. W.; Andrew, C. R.; Sanders-Loehr, J.; Bender, C. J.; Peisach, J. *Eur. J. Biochem.* **1993**, *218*, 229–238.
- (15) St Clair, C. S.; Ellis, W. R. J.; Gray, H. B. *Inorg. Chim. Acta* **1991**, *191*, 149–155.
- (16) Kalverda, A. P.; Ubbink, M.; Gilardi, G.; Wijmenga, S. S.; Crawford, A.; Jeuken, L. J. C.; Canters, G. W. *Biochemistry* **1999**, *38*, 12690–12697.
- (17) Bashford, D.; Karplus, M.; Canters, G. W. *J. Mol. Biol.* **1988**, *203*, 507–510.
- (18) Ben-Naim, A. *Cooperativity and Regulation in Biochemical Processes*; Kluwer Academic/Plenum: New York, 2001.
- (19) Ullmann, R. T.; Ullmann, G. M. GMCT—Monte Carlo Simulation Software for Macromolecular Receptors with Multiple Ligands, Membrane Potential and Conformational Flexibility. Submitted for publication.
- (20) Lapin, G. A.; Segal, M. G.; Weatherburn, D. C.; Henderson, R. A.; Sykes, A. G. *J. Am. Chem. Soc.* **1979**, *101*, 2302–2306.
- (21) Jeuken, L. J. C.; Wisson, L.-J.; Armstrong, F. A. *Inorg. Chim. Acta* **2002**, *331*, 216–223.
- (22) (a) Korzhnev, D. M.; Karlsson, V. Y.; Orekhov, B. G.; Billeter, M. *Protein Sci.* **2003**, *12*, 56–65. (b) Zhuraleva, A. V.; Korzhnev, D. M.; Kupce, E.; Arseniev, A. S.; Billeter, M.; Orekhov, V. Y. *J. Mol. Biol.* **2004**, *342*, 1599–1611.
- (23) Humphrey, W.; Dalke, A.; Schulten, K. *J. Mol. Graphics* **1996**, *14*, 33–38.
- (24) Stone, J. An Efficient Library for Parallel Ray Tracing and Animation, M.Sc. thesis, Computer Science Department, University of Missouri—Rolla, Rolla, MO, 1998
- (25) Ullmann, R. T.; Ullmann, G. M. Unpublished results.
- (26) Bashford, D. An object-oriented programming suite for electrostatic effects in biological molecules An experience report on the MEAD project. In *Scientific computing in object-oriented parallel environments*; Ishikawa, Y., Oldehoeft, R., Reynders, J., Tholburn, M., Eds.; Springer: Berlin/Heidelberg, Germany, 1997; Vol. 1343, pp 233–240.
- (27) Bashford, D. *Frontiers in Bioscience* **2004**, *9*, 1082–1099.
- (28) Becker, T.; Ullmann, R. T.; Ullmann, G. M. *J. Phys. Chem. B* **2007**, *111*, 2957–2968.
- (29) Ferreira, A. M.; Bashford, D. *J. Am. Chem. Soc.* **2006**, *128*, 16778–16790.
- (30) Gunner, M. R.; Mao, J.; Song, Y.; Kim, J. *Biochim. Biophys. Acta* **2006**, *1757*, 942–968.
- (31) Nielsen, J. E.; McCammon, J. A. *Protein Sci.* **2003**, *12*, 1894–1901.
- (32) Ullmann, G. M.; Knapp, E. W. *Eur. Biophys. J.* **1999**, *28*, 533–551.
- (33) Ullmann, G. M.; Kloppmann, E.; Essigke, T.; Krammer, E.-M.; Klingenberg, A. R.; Becker, T.; Bombarda, E. *Photosynth. Res.* **2008**, *97*, 33–53.
- (34) (a) te Velde, G.; Bickelhaupt, F. M.; Baerends, E. J.; Fonseca Guerra, C.; van Gisbergen, S. J. A.; Snijders, J. G.; Ziegler, T. *J. Comput. Chem.* **2001**, *22*, 931–967. (b) Fonseca Guerra, C.; Snijders, J. G.; te Velde, G.; Baerends, E. J. *Theor. Chem. Acc.* **1998**, *99*, 391–403.
- (35) Vosko, S. H.; Wilk, L.; Nusair, M. *Can. J. Phys.* **1980**, *58*, 1200–1211.
- (36) Swart, M.; Ehlers, A. W.; Lammertsma, K. *Mol. Phys.* **2004**, *102*, 2467–2474.
- (37) Swart, M.; van Duijnen, P. Th.; Snijders, J. G. *J. Comput. Chem.* **2001**, *22*, 79–88.
- (38) Becke, A. D. *Phys. Rev. A* **1988**, *38*, 3098–3100.
- (39) Perdew, J. P.; Yue, W. *Phys. Rev. B* **1986**, *33*, 8800–8802.
- (40) Lopez, X.; Schaefer, M.; Dejaegere, A.; Karplus, M. *J. Am. Chem. Soc.* **2002**, *124*, 5010–5018.
- (41) Brünger, A. T.; Karplus, M. *Proteins* **1988**, *4*, 148–156.
- (42) Brooks, B. R.; Bruccoleri, R. E.; Olafson, B. D.; States, D. J.; Swaminathan, S.; Karplus, M. *J. Comput. Chem.* **1983**, *4*, 187–217.
- (43) MacKerell, A. D.; Bashford, D.; Bellott, M.; Dunbrack, R. L.; Evanseck, J. D.; Field, M. J.; Fischer, S.; Gao, J.; Guo, H.; Ha, S.; et al. *J. Phys. Chem. B* **1998**, *102*, 3586–3616.
- (44) (a) Dunbrack, R. L. J.; Cohen, F. E. *Protein Sci.* **1997**, *6*, 1661–1681. (b) Dunbrack, R. L. J. *Curr. Opin. Struct. Biol.* **2002**, *12*, 431–440.
- (45) Bashford, D.; Karplus, M. *Biochemistry* **1990**, *29*, 10219–10225.
- (46) Bashford, D.; Case, D. A.; Dalvit, C.; Tennant, L.; Wright, P. E. *Biochemistry* **1993**, *32*, 8045–8056.
- (47) Klapper, I.; Fine, R.; Sharp, K. A.; Honig, B. H. *Proteins* **1986**, *1*, 47–59.
- (48) (a) Georgescu, R. E.; Alexov, E. G.; Gunner, M. R. *Biophys. J.* **2002**, *83*, 1731–1748. (b) Song, Y.; Mao, J.; Gunner, M. R. *J. Comput. Chem.* **2009**, *30*, 2231–2247.
- (49) Goldstein, R. F. *Biophys. J.* **1994**, *66*, 293–324.
- (50) (a) Wang, F.; Landau, D. P. *Phys. Rev. Lett.* **2001**, *86*, 2050–2053. (b) Wang, F.; Landau, D. P. *Phys. Rev. E* **2001**, *64*, No. 056101.
- (51) Metropolis, N.; Rosenbluth, A. W.; Rosenbluth, M. N.; Teller, A. H. *J. Chem. Phys.* **1953**, *21*, 1087–1092.
- (52) Zwanzig, R. W. *J. Chem. Phys.* **1954**, *22*, 1420–1426.
- (53) Ullmann, R. T.; Ullmann, G. M. *J. Phys. Chem. B* **2011**, *115*, 507–521.
- (54) Valleau, J. P.; Card, D. N. *J. Chem. Phys.* **1972**, *57*, 5457–5462.
- (55) Bennett, C. H. *J. Comput. Phys.* **1976**, *22*, 245–268.
- (56) Corin, A. F.; Bersohn, R.; Cole, P. E. *Biochemistry* **1983**, *22*, 2032–2038.
- (57) Uğurbil, K.; Mitra, S. *Proc. Natl. Acad. Sci. U. S. A.* **1985**, *82*, 2039–2043.
- (58) Monari, S.; Battistuzzi, G.; Dennison, C.; Borsari, M.; Ranieri, A.; Siwek, M. J.; Sola, M. *J. Phys. Chem. C* **2010**, *114*, 22322–22329.
- (59) van Pouderoyen, G.; Mazumdar, S.; Hunt, N. I.; Hill, A. O.; Canters, G. W. *Eur. J. Biochem.* **1994**, *222*, 583–588.
- (60) Battistuzzi, G.; Borsari, M.; Canters, G. W.; de Waal, E.; Loschi, L.; Warmerdam, G.; Sola, M. *Biochemistry* **2001**, *40*, 6707–6712.

- (61) Pascher, T.; Bergström, J.; Malmström, B. G.; Vännård, T.; Lundberg, L. G. *FEBS Lett.* **1989**, *258*, 266–268.
- (62) Pascher, T.; Karlsson, B. G.; Nordling, M.; Malmström, B. G.; Vännård, T. *Eur. J. Biochem.* **1993**, *212*, 289–296.
- (63) Pettigrew, G. W.; Leitch, F. A.; Moore, G. R. *Inorg. Chim. Acta* **1983**, *331*, 216–223.
- (64) (a) Hill, J. C.; Allen, H.; Leer, O.; Smith, B. E.; Ambler, R. P. *Biochem. Biophys. Res. Commun.* **1976**, *70*, 331–338. (b) Hill, H. A. O.; Smith, B. E. *J. Inorg. Biochem.* **1979**, *11*, 79–93.
- (65) (a) Uğurbil, K.; Norton, R. S.; Allerhand, A.; Bersohn, R. *Biochemistry* **1977**, *16*, 886–894. (b) Uğurbil, K.; Bersohn, R. *Biochemistry* **1977**, *16*, 3016–3023.
- (66) van de Kamp, M.; Hali, F. C.; Rosato, N.; Agro, A. F.; Canters, G. W. *Biochim. Biophys. Acta, Bioenerg.* **1990**, *1019*, 283–292.
- (67) Simonson, T. *Curr. Opin. Struct. Biol.* **2001**, *11*, 243–252.
- (68) Webb, H.; Tynan-Connolly, B. M.; Lee, G. M.; Farrell, D.; O'Meara, F.; Søndergaard, C. R.; Teilum, K.; Hewage, C.; McIntosh, L. P.; Nielsen, J. E. *Proteins* **2010**, *79*, 685–702.
- (69) (a) Wilson, M. T.; Greenwood, C.; Brunori, M.; Antonini, E. *Biophys. J.* **1975**, *14S*, 449–457. (b) Wilson, M. T.; Greenwood, C.; Brunori, M.; Antonini, E. *Biophys. J.* **1975**, *15I*, 185–188.
- (70) Ullmann, G. M. *J. Phys. Chem. B* **2000**, *104*, 6293–6301.
- (71) Bombarda, E.; Ullmann, G. M. *J. Phys. Chem. B* **2010**, *114*, 1994–2003.
- (72) Ullmann, G. M. *J. Phys. Chem. B* **2003**, *107*, 1263–1271.
- (73) Carter, P. J.; Winter, G.; Wilkinson, A. J.; Fersht, A. R. *Cell* **1984**, *38*, 835–840.
- (74) Horovitz, A. *Folding Des.* **1996**, *1*, R121–R126.
- (75) Onufriev, A.; Case, D. A.; Ullmann, G. M. *Biochemistry* **2001**, *40*, 3413–3419.
- (76) Spassov, V.; Bashford, D. *Protein Sci.* **1998**, *7*, 2012–2025.
- (77) Silvestrini, M. C.; Brunori, M.; Wilson, M. T.; Darley-Uzman, V. M. J. *Inorg. Biochem.* **1981**, *14*, 327–338.
- (78) Ubbink, M. *FEBS Lett.* **2009**, *583*, 1060–1066.
- (79) Jeuken, L. J. C. *Biochim. Biophys. Acta, Bioenerg.* **2003**, *1604*, 67–76.
- (80) (a) Davidson, V. L. *Biochemistry* **1996**, *35*, 14036–14039. (b) Davidson, V. L. *Biochemistry* **2000**, *39*, 4924–4928. (c) Davidson, V. L. *Biochemistry* **2002**, *41*, 14633–14636.
- (81) Farver, O.; Blatt, Y.; Pecht, I. *Biochemistry* **1982**, *21*, 3556–3561.
- (82) van de Kamp, M.; Floris, R.; Hali, F. C.; Canters, G. W. *J. Am. Chem. Soc.* **1990**, *112*, 907–908.
- (83) (a) van Amsterdam, I. M. C.; Ubbink, M.; Jeuken, L. J. C.; Verbeet, M. P.; Einstle, O.; Messerschmidt, A.; Canters, G. W. *Chem.—Eur. J.* **2001**, *7*, 2398–2406. (b) van Amsterdam, I. M. C.; Ubbink, M.; Jeuken, L. J. C.; Verbeet, M. P.; Einstle, O.; Messerschmidt, A.; Canters, G. W. *Nat. Struct. Biol.* **2002**, *9*, 48–52. (c) van Amsterdam, I. M. C.; Ubbink, M.; Canters, G. W. *Inorg. Chim. Acta* **2002**, *331*, 296–392.
- (84) Sokerina, E. V.; Ullmann, G. M.; van Pouderoyen, G.; Canters, G. W.; Kostic, N. M. *J. Biol. Inorg. Chem.* **1999**, *4*, 111–121.
- (85) Xu, C.; Yin, J.; Zhao, B. *Sci. China, Ser. C: Life Sci.* **2010**, *53*, 1181–1188.
- (86) Dumit, V. I.; Essigke, T.; Cortez, N.; Ullmann, G. M. *J. Mol. Biol.* **2010**, *397*, 814–825.
- (87) Zhu, Z.; Cunane, L. M.; Chen, Z.; Durley, R. C. E.; Mathews, F. S.; Davidson, V. L. *Biochemistry* **1998**, *37*, 17128–17136.
- (88) Tordi, M. G.; Silvestrini, M. C.; Colosimo, A.; Tuttobello, L.; Brunori, M. *Biochem. J.* **1985**, *230*, 797–805.
- (89) Silvestrini, M. C.; Falcinelli, S.; Ciabatti, I.; Cutruzzolà, F.; Brunori, M. *Biochimie* **1994**, *76*, 641–654.
- (90) Vollack, K.-U.; Xie, J.; Härtig, E.; Römling, U.; Zumft, W. G. *Microbiol.* **1997**, *143*, 2853–2863.
- (91) Hasegawa, N.; Arai, H.; Igarashi, Y. *Biochim. Biophys. Res. Commun.* **2001**, *288*, 1223–1230.
- (92) Barber, D.; Parr, S. R.; Greenwood, C. *Biochem. J.* **1961**, *157*, 431–438.
- (93) Amunts, A.; Nelson, N. *Structure* **2009**, *17*, 637–650.
- (94) Fromme, R.; Grotjohann, I.; Fromme, P. Structure of Photosystems I and II. In *Structural Biology of Membrane Proteins*; Grissamer, R., Buchanan, S. K., Eds.; The Royal Society of Chemistry: London, 2006; Chapter 18, pp 320–348.
- (95) Rogers, L. J. *Ferredoxins, Flavodoxins, and Related Proteins: Structure, Function, and Evolution*. In *Cyanobacteria: A Comprehensive Review*; Fay, P., van Baalen, C., Eds.; Elsevier: Amsterdam, The Netherlands, 1987; pp 35–67.
- (96) Ullmann, G. M. *Simulation and Analysis of Docking and Molecular Dynamics of Electron-Transfer Protein Complexes*, Ph.D. thesis, Freie Universität Berlin, Berlin, 1998.
- (97) Ullmann, G. M.; Hauswald, M.; Jensen, A.; Kostic, N. M.; Knapp, E. W. *Biochemistry* **1997**, *36*, 16187–16196.
- (98) Ullmann, G. M.; Hauswald, M.; Jensen, A.; Knapp, E. W. *Proteins* **2000**, *38*, 301–309.
- (99) Poole, R. K.; Cook, G. M. *Redundancy of Aerobic Respiratory Chains in Bacteria? Routes, Reasons and Regulation*. In *Advances in Microbial Physiology*; Poole, R. K., Ed.; Academic Press: New York, 2000; Vol. 43, pp 165–224.
- (100) Matsushita, K.; Yamada, M.; Shinagawa, E.; Adachi, O.; Ameyama, M. *J. Bacteriol.* **1980**, *141*, 389–392.
- (101) Stover, C. K.; Pham, X. Q.; Erwin, A. L.; Mizoguchi, S. D.; Warrener, P.; Hickey, M. J.; Brinkman, F. S. L.; Hufnagle, W. O.; Kowalik, D. J.; Lagrou, M.; et al. *Nature* **2000**, *406*, 959–964.
- (102) Williams, P. A.; Fulop, V.; Leung, Y.-C.; Chan, C.; Moir, J. W. B.; Howlett, G.; Ferguson, S. J.; Radford, S. E.; Hajdu, J. *Nat. Struct. Biol.* **1995**, *2*, 975–982.
- (103) Okamura, M. Y.; Paddock, M. L.; Graige, M. S.; Feher, G. *Biochim. Biophys. Acta, Bioenerg.* **2000**, *1458*, 148–163.
- (104) Renger, G.; Renger, T. *Photosynth. Res.* **2008**, *98*, 53–80.
- (105) Chakrabarty, S.; Namslauer, I.; Brzezinski, P.; Warshel, A. *Biochim. Biophys. Acta, Bioenerg.* **2011**, *1807*, 413–426.
- (106) Capitanio, G.; Martino, P. L.; Capitanio, N.; Papa, S. *Biochim. Biophys. Acta, Bioenerg.* **2011**, in press (DOI: 10.1016/j.bbabi.2011.02.004).
- (107) Mulkidjanian, A. Y. *Biochim. Biophys. Acta, Bioenerg.* **2010**, *1797*, 1858–1868.
- (108) Crofts, A. R. *Annu. Rev. Physiol.* **2004**, *66*, 689–733.
- (109) Hunte, C.; Palsdottir, H.; Trumper, B. *FEBS Lett.* **2003**, *545*, 39–46.